SLAC–PUB–7659
OCT 1997

Photocathode Guns for Single Pass X-ray FELs*

D. T. Palmer

Stanford Linear Accelerator Center
Stanford University
Stanford, CA 94309

Abstract

The present state of the art in photoinjector designs will be presented in this review. We will discuss both proposed and operational photoinjectors with operating frequencies from L-band (1.424 GHz) to X-band (11.424 GHz). Also a novel pulsed DC gun will be presented. All the RF photoinjector discussed here use an emittance compensation scheme [1] [2] to align the different slices of the the electron beam to decrease the beams normalized rms emittance.

Invited paper presented at
Workshop on Single Pass, High Gain FELs starting from Noise,
aiming at Coherent X-rays - Toward X-ray Free Electron Lasers
Gargnano, Italy
2-7 June 1997

*Work supported by Department of Energy contract DE–AC03–76SF00515, DE-AC02-76CH00016 and DE-FG03-92ER40793.

Photocathode Guns for Single Pass X-ray FELs[†]

D. T. Palmer
Stanford Linear Accelerator Center
2575 Sand Hill Road
Stanford, California 94309

Abstract

The present state of the art in photoinjector designs will be presented in this review. We will discuss both proposed and operational photoinjectors with operating frequencies from L-band (1.424 GHz) to X-band (11.424 GHz). Also a novel pulsed DC gun will be presented. All the RF photoinjector discussed here use an emittance compensation scheme [1] [2] to align the different slices of the the electron beam to decrease the beams normalized rms emittance.

1 PROPOSED PHOTOINJECTORS

1.1 Pulsed DC Photoinjector

A pulsed DC photoinjector [3] has been proposed with an accelerating gradient of 1 $\frac{\mathrm{GV}}{\mathrm{m}}$. Beam dynamics simulations indicate that this design can achieve substantial lower normalized rms emittance than is achievable with rf photoinjectors.

1.2 L-Band Radio Frequency Photoinjectors

A proposed injector for the TESLA Test Facility(TTF) has eliminate the RF power feed constraint by used a door knob coupler [4]. This novel power coupler design therefore allows for the positioning of the emittance compensation magnet in the optimum position for its design. A second photoinjector designed, built and tested for the TTF is the FERMI Lab A0 photoinjector which has worked around the rf power feed constraint problem by using a split emittance compensation magnet design [5].

1.3 X-Band Radio Frequency Photoinjectors

The push to higher gradients in RF guns has spurred the development of a 11.5 cell integrated photoinjector based on the PWT accelerator design at UCLA [6]. This gun runs at a peak field of 240 $\frac{\mathrm{MV}}{\mathrm{m}}$ and is capable of attaining a normalized rms emittance of less than 1.00 π mm mrad for a total bunch charge of 1 nC.

2 OPERATIONAL PHOTOINJECTORS

2.1 S-Band Photoinjectors

The proposed photoinjector [7] for the Linear Coherent Light Source(LCLS) [8] at the Stanford Linear Accelerator Center is the BNL/SLAC/UCLA 1.6 cell Symmetrized S-Band Emittance Compensated RF gun and emittance compensation magnet. This RF gun has been designed to reduce the RF dipole mode contribution in the electron beam normalized rms emittance, $\epsilon_{\mathrm{n,rms}}$ [9]. The RF power feed into the full cell of this gun constrains the positioning of the emittance compensation magnet. PARMELA [10] simulations indicate that there can be a 15% improvement in injector performance with the elimination of this mechanical constraint [11].

3 BEAM DYNAMICS STUDIES

We shall present beam dynamics studies of the BNL/SLAC/UCLA 1.6 cell Symmetrized S-Band Emittance Compensated RF Gun, which is the prototype for the LCLS RF gun. The beam dynamics results presented here were conducted at the Brookhaven National Laboratory Accelerator Test Facility with a final beam energy of 40 MeV.

3.1 Low Charge Emittance Measurements [12]

PARMELA was used to simulate the emittance compensation process and the subsequent acceleration to 40 MeV. A correlation of the minimum spot size with an emittance minimum was noted during these simulations. This was experimentally verified during the commissioning of the 1.6 cell rf gun, using the beam profile monitor located at the output of the second linac section, as can be seen in figure 1. The result in figure 1 is for a total bunch charge of 0.329 ± 0.012 nC, an electron bunch length of $\tau_{95\%} = 10.9$ psec with an $\epsilon_{\mathrm{n,rms}} = 1.17 \pm 0.16$ π mm mrad.

The dependence of transverse emittance on the bunch charge under two different experimental conditions are presented in figure 2. The linear dependent emittance versus charge was conducted under constant solenoidal magnet field that was optimized for a total charge of 390 pC and only the laser energy on the cathode was varied. For the quadratic dependent emittance versus charge, as the laser energy was varied the beam was optimized using the solenoidal magnet and steering magnets to produce the smallest symmetric beam profile at the first high energy profile screen. Note that even under these diverse experimental condition the measured emittance are consistent with the data in figure 1.

For the quadratic dependent emittance versus charge experiment it is clear that the beam line tune is not satisfac-

[†] Work supported by the Department of Energy, contracts DE-AC03-76SF00515, DE-AC02-76CH00016 and DE-FG03-92ER40793

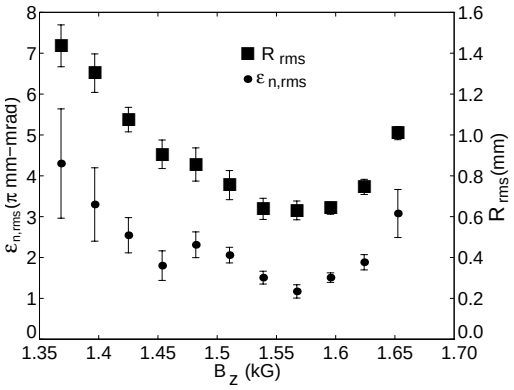

Figure 1: $\epsilon_{\mathrm{n,rms}}$ and $\mathrm{R_{rms}}$ versus $\mathrm{B_{z,max}}$

tory. This experiment points out an defect in beam line tuning, in that tuning for best emittance is not that same as tuning for the best spot size. Advanced diagnostics must tune for emittance and not spot size quality which is a qualitative beam feature.

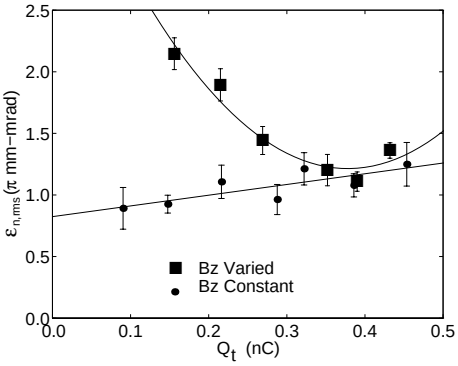

Figure 2: $\epsilon_{\mathrm{n,rms}}$ versus $\mathrm{Q_t}$

3.2 Cathode Magnet Field Emittance Contribution [11]

Due to the single emittance compensation solenoidal magnet a small but finite field at the rf gun cathode the electron bunch are produced with a finite angular momentum. We have measured the relative angular rotation due to this finite field. In this experiment a 8-fold symmetric mask [13] [14] was inserted into the the laser beam thereby producing the laser profile on the cathode shown in figure 3.

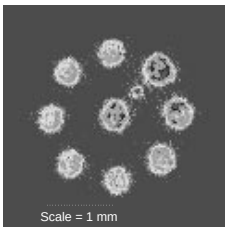

Figure 3: 8 fold symmetric beamlets

The smallest beamlet located at 45° is used to break the symmetry. In this way we were able to measure the betatron rotation of the beam thru the solenoidal magnet which was found to be approximately 90°. The 8-fold beamlet relative angular rotation was measured as a function of bucking magnet field for point to point imaging of the 8-fold beamlets from the cathode to a beam profile monitor located 66.4 cm from the cathode. Figure 4 represents the relative angular rotation of the 8-fold symmetric beamlets due to the cathode magnetic field and has a linear dependence.

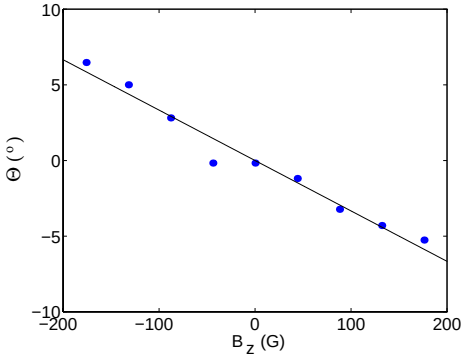

Figure 4: $\Phi_{\mathrm{rel}}(\mathrm{z}=0)$ versus $\mathrm{B_z}(\mathrm{z}=0)$

The rms spot size as a function of cathode magnet field was measured with a beam energy of 40 MeV. The dependence of the high energy spot size with respect to cathode magnetic field is shown in figure 5. This data indicates that the minimum spot size occurs with a cathode magnetic field of -5 G. The cathode field with the bucking magnet off is +4 G. These results indicate that the cathode field can not be zeroed better than the mechanical construction and alignment of the photoinjector itself.

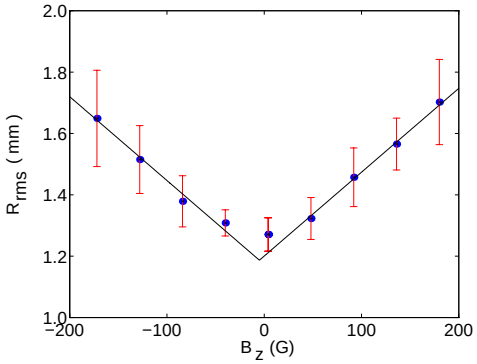

Figure 5: High energy $\mathrm{R_{rms}}$ versus $\mathrm{B_z}(\mathrm{z}=0)$

Due to experimental instabilities it was not possible to measure the emittance growth due to the induced cathode magnetic field. From the spot size variation at high energy due to the induced cathode magnetic field and the correlation between spot size and measured $\epsilon_{\mathrm{n,rms}}$ [11], the emittance growth as a function of cathode magnetic field can be estimated. In table 1 the correlated experimental results of $\epsilon_{\mathrm{n,rms}}$ growth as a function of induced cathode mag-

Experimental Result	$0.010 \frac{\pi \text{ mm}-\text{mrad}}{\text{G}}$
PARMELA	$0.006 \frac{\pi \text{ mm}-\text{mrad}}{\text{G}}$
THEORY	$0.007 \frac{\pi \text{ mm}-\text{mrad}}{\text{G}}$

Table 1: Comparison of experimental results, simulation and theory for the emittance growth due to the cathode magnetic field

netic field is presented along with PARMELA simulation and theoretical [15] predications.

3.3 RF Field Asymmetry Emittance Contribution [16]

Phase variations in the rf gun, due to rf breakdown in the TEM coaxial conductor, prevented measurement of emittance growth due to gun disymmetrization from being conducted.

In the either mode of operation, the 8-fold beamlets were point to point focused, using the single emittance compensation magnet [11], to a beam-profile monitor screen located 66.4 cm from the cathode plane. The center beamlet profile in figures 6 and 7 represent the beamlet profiles in the symmetric and asymmetric mode of operation respectively, with the central beamlet on the geometric center of the rf gun. Mechanical alignment and dark current studies indicate that the geometrical and integrated electrical centers of the rf gun are with in 50μm of each other in the symmetrized mode. Steering the laser beam $\pm$ 1 mm on the x and y axis we are able to probe the electromagnetic field in the 1.6 cell rf gun out to a radius of approximately 2.4 mm and produce the eight additional images in both figures 6 and 7. It should be noted that the betatron rotation of the solenoidal magnet has been removed numerical from these images so that a direct comparison of the individual beamlet position and distortion can be directly compared to the full cells cavity penetrations.

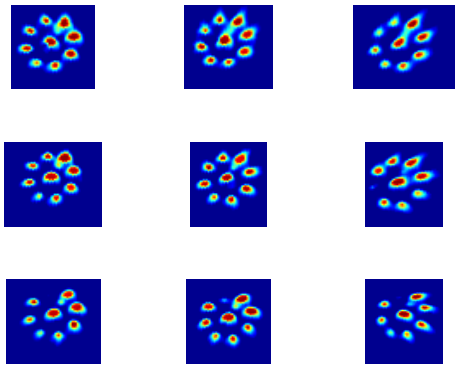

Figure 6: Beamlets profile with rf gun symmetrized

In the analysis of the center 8-fold beamlets in figures 6 and 7 for the symmetrized and unsymmetrized mode of operation we have seem no centroid deflection for the outer ring of beamlets with respect to the on axis beamlet, as is expected since the TM_{110} magnetic field is uniform in

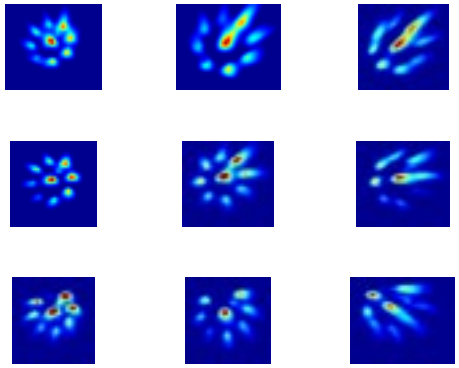

Figure 7: Beamlets profile with the rf gun unsymmetrized

the beam region of the cavity. This effect is seem in figure 8. The difference in total deflection between the different modes of operation is due to the peak rf field that the rf gun could hold off was lower in the unsymmetrized cases, since the vacuum/plunger TEM coaxial conductor would breakdown at the higher rf fields used in the symmetrized mode of operation. The normalized deflection in both modes are approximately the same.

The effect of the symmetrized versus unsymmetrized mode of operation can be seem in figure 9. This figure represents the individual beamlets Full Width Tenth Maximum (FWTM) profiles. The data that represents the unsymmetrized mode of operation has a dominate dipole mode contribution as would be expected. In the symmetrized case the dipole contribution is minimized with the dominate mode being the quadrupole contribution, as would be expected from theory. Analyses is ongoing to fully understand this effect.

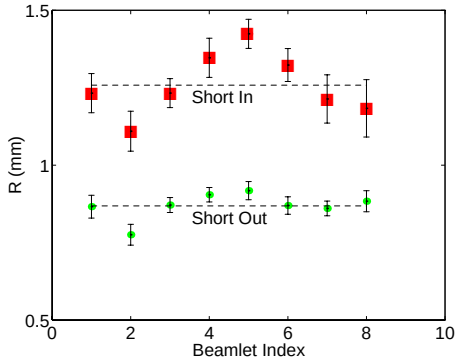

Figure 8: Beamlet centroid position from center beamlet

Multi-pole field effects were also studied by decreasing the laser spot size to 400 μm and setting the laser injection phase to the Schottky peak. This injection phase causes an effective electron bunch-lengthening and a noticeable energy-spread tail was observed. By adjusting the laser spot position we were able to eliminate this energy spread tail. This alignment minimizes the integrated higher-order-mode contribution to the beam distortion. Analysis indicates that the symmetrized BNL/SLAC/UCLA 1.6 cell

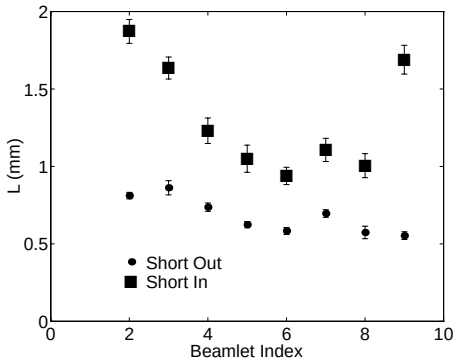

Figure 9: Individual beamlet radial extent

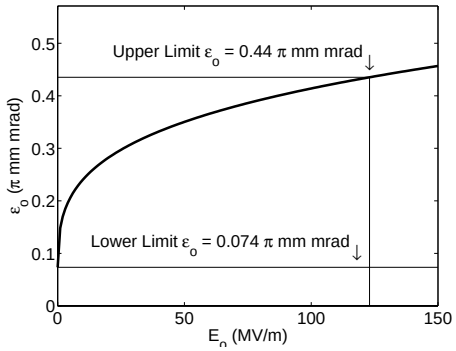

Figure 10: Thermal emittance, $\epsilon_{\rm o}$, as a function of cathode field

photocathode rf gun's electrical and geometric center are within 170 μm of each other, which is within the laser spot alignment error of 250 μm. Compared to similar experimental results of the 1.5 cell BNL gun [17] whose electrical and geometric centers differ by 1.0 mm, the 1.6 cell gun has fulfilled the symmetrization criteria.

3.4 Thermal emittance Contribution

We have noted that at Q=0 for the linear dependence emittance versus charge there is a residual emittance term of 0.8 π mm-mrad. This term is due to $\epsilon_{\rm o}$, $\epsilon_{\rm rf}$ and $\epsilon_{\rm mag}$. The magnetic term can be neglected since the initial cathode spot size and the small magnetic field at the cathode will contribute only 0.03 π mm mrad [11]. The rf contribution should be small, since there is no transverse space charge forces to cause beam size expansions in the rf gun. The beam, in this limiting charge case, will only sample a small portions of the rf fields which decrease the rf contribution by $\sigma_{\rm x}^2$ [18]. The beams intrinsic thermal emittance including the Schottky correction is given in equation 1. A theoretical estimate of the thermal emittance at 125 $\frac{\rm MV}{\rm m}$ for a copper cathode was found to be 0.44 π mm-mrad.

$$\epsilon_o \;\leq\; 0.8\,\pi\,\mathrm{mm\ mrad} \tag{1}$$

The beam thermal emittance is given by equation 2.

$$\epsilon_{\rm o} \;=\; \frac{\rm r}{2}\sqrt{\frac{\rm kT}{\rm mc^2}} \tag{2}$$

Where the term kT is given by the difference between the laser photon energy and the effective work function of the cathode material. The effective work function of the cathode material is given by

$$\phi \;=\; \phi_{\rm o} \;-\; \sqrt{\beta\,{\rm E_o}\,\sin(\theta)} \tag{3}$$

where ϕ is the work function of the material under high gradient, $\phi_{\rm o}$ is the zero field work function and β is the optically polished photo-emitting areas field enhancement factor. The dependence of the beams thermal emittance is shown in figure 10 as a function of field gradient.

the experimental data in the zero charge limit with the upper limit of the theoretical calculation lends credence to our Schottky corrected thermal emittance value for the Cu cathode of $\epsilon_{\rm o} \;=\; 0.44\,\pi\,\mathrm{mm\ mrad}$.

An interesting ideas to eliminate the thermal emittance contribution or at least decrease its effect is to design the photoemission process in such a way to take advantage of the Schottky effect. By this I mean the system should be designed with a cathode material with a higher work function than that of the laser photon energy. With an appropriate cathode field that has been chosen to optimized the emittance compensation process, the effective work function of the material would be less than that of the laser photon energy by some small but finite amount. In this way the excess electron can be tuned by the accelerating field such that this excess energy is zero.

Also the use of a spin polarized rf gun operating in the emittance compensation regime would allow for the production of an emittance compensation electron beam with a zero thermal emittance contribution. Since the production of a spin polarized electron beam necessitates that the photon energy be tune to the band gap energy there should be no excess electron energy that could manifest itself into a thermal emittance term. It should be pointed out that this would not be the case is a negative electron affinity photocathode were used since in these cathode materials the vacuum energy level is less than that of the conduction band minimum.

It should be pointed out that both of these proposed methods make the available laser power an important parameter since we are not depending on the Schottky effect or the NEA to increase the quantum efficiency of the photocathode material. Also of possible importance is the time dependent variation of the band structure of the GaAs due the large applied time depend electromagnetic field.

3.5 High Charge Emittance Measurements [12]

For X-ray free electron laser application such as the Linear Coherent Light Source(LCLS) the relevant photoinjector parameters are 1 nC, $\tau_{95\%} = 10$ psec and 1.00 π mm mrad normalized rms emittance. The measured and LCLS values are presented in table 2.

Parameter	LCLS	Experimental Results
Q_T	1 nC	1.020 ± 0.059 nC
$\tau_{95\%}$	10 psec	14.7 psec
$\epsilon_{\mathrm{n,rms}}$	1.00 π mm mrad	4.74 ± 0.24 π mm mrad

Table 2: 1 nC emittance results

Simulation results using PARMELA with a longitudinal flat top electron pulse of $\tau_{95\%} = 10$ psec, full width tenth maximum (FWTM), indicate that a $\epsilon_{\mathrm{n,rms}} \leq 1$ π mm mrad is attainable [19].

The results of our experimental studies present two challenges. First is the increased $\tau_{95\%}$ and second is the larger than expected $\epsilon_{\mathrm{n,rms}}$. These are not unrelated since the emittance contribution due to rf scales as σ_z^2. Therefore an important issue is to find the mechanism causing the electron bunch length to increase. Two possible mechanisms were studied; laser pulse bunch lengthening due to laser power saturation in a doubling crystal, or space charge bunch lengthening. Experimental studies of the correlation of the laser power and $\tau_{95\%}$ were undertaken. Figure 11 shows the results of these studies. While keeping the total electron bunch charge constant at 360 pC, the laser intensity in the green(λ = 532 nm) was increased. The results is that $\tau_{95\%}$ = 10.9 psec. Keeping the laser intensity in the green constant and varying the uv on the cathode to increase the electron bunch charge from 400 pC to 1nC results in an increase in the $\tau_{95\%}$ from 10.9 psec to 14.7 psec (Figure 11). This clearly shows that the 1 nC electron bunch length is not due to the laser pulse length but due to some beam dynamics issue, almost surely longitudinal space charge forces.

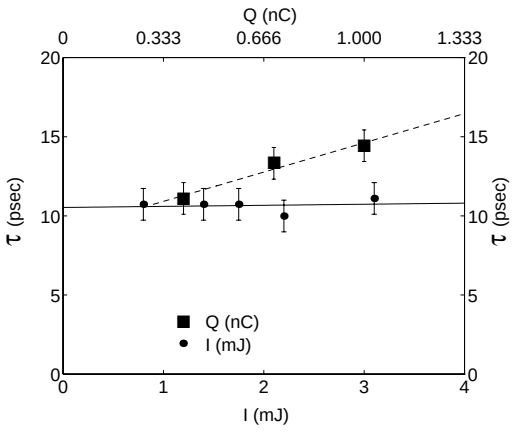

Figure 11: $\tau_{95\%}$ versus $\mathrm{I_{green}}$ with $\mathrm{Q_t}$ constant. $\tau_{95\%}$ versus $\mathrm{Q_t}$ with $\mathrm{I_{green}}$ constant.

PARMELA simulation do not show the space charge bunch lengthening seen in these experiments and this simulation error is being investigated. A group was formed at PAC97 to cross check the validty of different space charge dominated beam dynamics codes with respect to each other and with the experimental results of the BNL/SLAC/UCLA 1.6 cell S-band emittance compensated RF gun.

Before Laser Cleaning	
Q_t	918 ± 77.5 pC
$\epsilon_{\mathrm{n,rms}}$	5.18 ± 0.25 π mm mrad
After Laser Cleaning	
Q_t	1020 ± 58.7 pC
$\epsilon_{\mathrm{n,rms}}$	4.74 ± 0.24 π mm mrad

Table 3: High charge emittance study results before and after LAEEE

This debunching effect due to space charge forces can be corrected by decreasing the laser pulse length and using the debunching effect to lengthen the $\tau_{95\%}$ to the required 10 psec. This technique has the drawback the longitudinal phase mixing of the electron pulse could possible occur thereby degrading the emittance compensation process. A second possibility is to increase the laser spot size. But this would increase the emittance due to the rf emittance contribution, the remnant magnetic field at the cathode and also increase the intrinsic thermal emittance. Using a longitudinally flat top laser pulse would seem to be the best solution since the magnetic and thermal emittance would not increase and the longitudinal space charge forces would be decreased in the central portion of the bunch.

Due to the non-uniformity of the transverse laser pulse and transverse variation of the cathode quantum efficiency, the electron bunch transverse charge density $\rho(\mathrm{x},\mathrm{y})$ is not uniform. Laser assisted explosive electron emission(LAEEE) [20] has been used to smooth out this effect. The measured improvement in $\epsilon_{\mathrm{n,rms}}$ due to LAEEE are presented in table 3. Qualitative data for $\mathrm{QE}(\mathrm{x},\mathrm{y})$ of the copper cathode is not available, but for the magnesium cathode LASEEE improved the $\mathrm{QE}(\mathrm{x},\mathrm{y})$ by a factor of two, from an order of magnitude variation across the cathode spot to a 50% after LASEEE.

A proposed correction for the cathode QE variation problem has been suggested by the author. By measuring the energy variation of the transverse laser profile with a calibrated CCD and the transverse electron charge distribution with a n-pole strip line, a correction signal can be sent to an array of liquid crystal pixels, that is inserted into the laser beamline, to distort the lasers transverse energy distribution in such a manner that a given electron charge distribution is produced. This non-invasive feedback system is presented in figure 12.

It should be noted that by using another CCD to measure the 2D variation of the electron beam as is strikes a beam profile screen, we could eliminate the need for the feedback control system, but this method would be invasive and would require periodic transverse charge distribution to insure that the cathode properties are not varying on the time scale of the FEL run.

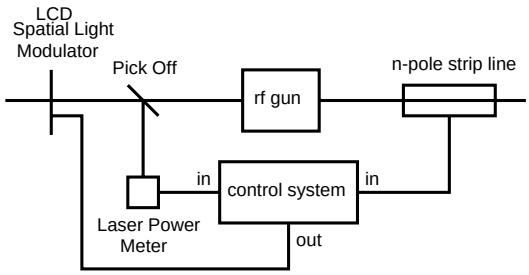

Figure 12: A non-invasive feedback system to correct for the 2D variation of the electron charge distribution.

3.6 Conclusion

The experimental results from the BNL/SLAC/UCLA 1.6 cell S-band emittance compensated RF gun has pointed out areas for future work. These include the experimental investigation of the thermal emittance contribution to the normalized rms emittance from Cu cathode materials. The photocathode materials group at INFN LASE Milano lead by Paolo Michelato, has agreeded to conduct zero field electron velocity distribution measurements on CU (100). These results will allow for an exact calculation of the thermal emittance contribution in the zero field limit. Two novel techniques for the reduction or elimination of the thermal emittance contribution to the normalized rms emittance have been presented. Also comparing different beam dynamics simulation codes for consistence with each other and with the experimental results is of critical importance and is ongoing.

4 ACKNOWLEDGMENT

The work presented here is the the product of years of work and I would like to thank Drs. Ilan Ben-Zvi, Bruce Carlsten, Kwang-Je Kim, Roger Miller, Claudio Pellegrini, James Rosenzweig, Luca Serafini, Richard Sheffield, Xi-Jie Wang and Herman Winick for their intellectual effort in the development of RF Photoinjector technology. The author would like to thank the technical staff at BNL, SLAC and UCLA for all their dedicated work during the design, construction, installation and commissioning of the BNL/SLAC/UCLA 1.6 cell symmetrized S-band emittance compensated RF photoinjector.

5 REFERENCES

[1] B. E. Carlsten, *NIM*, **A285**, 313 (1989)

[2] L. Serafini and J. B. Rosenzweig, Phys. Rev. E, **55**, 7565, (1997)

[3] T. Srinivasan-Rao *et al.*, Proc. 1996 Adv. Accel. Concepts Workshop

[4] K. Flotmann *et al.*, TTF-FEL Design Report

[5] E. Colby, *et al.*, Proc. 1997 Part. Accel. Conf., 4W.20

[6] J.B. Rosenzweig *et al.*, Proc. 1997 Part. Accel. Conf., 9V.33

[7] A. D. Yeremian *et al.*, Proc. 1997 Part. Accel. Conf., 4W.14

[8] H. Winick, *Electron Spectrosc. Relat. Phenom.*, **75**, 1-8 (1995)

[9] D. T. Palmer *et al.*, Proc. 1995 Part. Accel. Conf., SLAC-PUB-6799

[10] L. M. Young, private communications

[11] D. T. Palmer *et al.*, Proc. 1997 Part. Accel. Conf., 4W.10

[12] D. T. Palmer *et al.*, Proc. 1997 Part. Accel. Conf., 2C.10

[13] Z. Li, Ph.D. Thesis

[14] D. W. Feldman *et al.*, IEEE J. Quantum Electronic, **27**, 12, 2636-2643 (1991)

[15] K. Flotmann, private communications

[16] D. T. Palmer *et al.*, Proc. 1997 Part. Accel. Conf., 4W.11

[17] X. J. Wang *et al.*, Proc. 1995 Part. Accel. Conf. (1995) p. 890

[18] K. J. Kim, *NIM*, **A275**, 201 (1989)

[19] D. T. Palmer *et al.*, Proc. 1995 Part. Accel. Conf., SLAC-PUB-6800

[20] X. J. Wang *et al.*, J. Appl. Phys. 72(3), 888-894